First-passage times to anisotropic partially reactive targets

Adrien Chaigneau [*] and Denis S. Grebenkov [†]
Laboratoire de Physique de la Matière Condensée (UMR 7643), CNRS–Ecole Polytechnique, IP Paris, 91120 Palaiseau, France

(Received 18 March 2022; accepted 5 May 2022; published 25 May 2022)

We investigate restricted diffusion in a bounded domain towards a small partially reactive target in three- and higher-dimensional spaces. We propose a simple explicit approximation for the principal eigenvalue of the Laplace operator with mixed Robin-Neumann boundary conditions. This approximation involves the harmonic capacity and the surface area of the target, the volume of the confining domain, the diffusion coefficient, and the reactivity. The accuracy of the approximation is checked by using a finite-elements method. The proposed approximation determines also the mean first-reaction time, the long-time decay of the survival probability, and the overall reaction rate on that target. We identify the relevant lengthscale of the target, which determines its trapping capacity, and we investigate its relation to the target shape. In particular, we study the effect of target anisotropy on the principal eigenvalue by computing the harmonic capacity of prolate and oblate spheroids in various space dimensions. Some implications of these results in chemical physics and biophysics are briefly discussed.

DOI: 10.1103/PhysRevE.105.054146

I. INTRODUCTION

Diffusion-controlled reactions play a central role in various physical, chemical, and biological phenomena [1–10]. At a single-molecule level, these processes are characterized by the so-called first-passage time statistics. In a typical setting, a particle (e.g., a protein or an ion) diffuses inside a confining domain and searches for a specific target (e.g., an enzyme or a receptor) to react with. The distribution of the reaction time (i.e., the first time instance at which the reaction occurs) depends on the diffusive dynamics, the shapes of the domain and of the target, its reactivity, and its location with respect to the starting position of the diffusing particle [11–27]. While this distribution can in general be obtained by solving the Fokker-Planck equation with appropriate boundary conditions [3,28], such a solution remains too formal and not very informative, except for a few basic domains such as an interval, concentric circles, or spheres (see, e.g., [29]).

In the case of a *small* target, more explicit solutions are available. For instance, matched asymptotic methods can be employed to compute the mean first-passage time, the smallest eigenvalue of the governing Laplace operator, and other characteristics of diffusion-controlled reactions [30–41] (see also review [42] and references therein). By a different method based on pseudopotentials, Isaacson and Newby developed a uniform asymptotic approximation of diffusion to a small target [43]. When the target is located on the boundary, homogenization techniques can be applied [44–52] (see also the discussion in [53]). In some geometric settings, one can go further and develop self-consistent approximations for the mean reaction time and its whole distribution [54–58]. In the case of elongated domains, the original multidimensional setting can be reduced to an effective one-dimensional problem that admits explicit solutions [59,60].

When a small target is located inside a confining domain far from reflecting boundaries, the shape of the target is generally ignored. In fact, one often dealt with a spherical target, which is characterized by a single lengthscale—its diameter (or radius). Even if a small sphere was replaced by a small cube or a small disk of the same size, its reaction rate or trapping capacity for diffusing particles would be modified insignificantly (see, e.g., examples in [60]). Several former studies were dedicated to the impact of the target shape onto the trapping constant of diffusion-limited reactions [61–71] and, more recently, onto the mean first-passage time [55]. Despite these works, the role of target anisotropy in diffusion-controlled reactions remains poorly understood. In fact, if the target is elongated (e.g., cigar-shaped), there are at least two relevant geometric lengthscales, namely its "length" and "width," and identification of an appropriate "size" of the target is not clear. In particular, if the "length" is fixed but the "width" vanishes, such a degenerated target (a needle) becomes inaccessible to Brownian motion, i.e., its trapping constant vanishes. If the target is partially reactive [11,13,44,46,50,52–54,67,72–88], the anisotropy effect is even more sophisticated.

In this paper, we consider restricted diffusion in a bounded d-dimensional domain towards a small partially reactive target. We focus on the principal (smallest) eigenvalue λ_1 of the Laplace operator, which is related to the reaction or trapping rate and determines the mean first-reaction time and the decay rate of the survival probability (see below). We propose a simple approximation for λ_1, which exhibits an explicit dependence on the target reactivity. This approximation allows us to identify the proper trapping length of the target. To analyze the effect of target anisotropy, we will focus on

[*]adrien.chaigneau@protonmail.com
[†]denis.grebenkov@polytechnique.edu

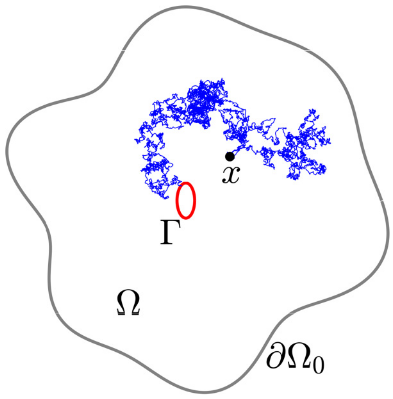

FIG. 1. A confining domain Ω with reflecting boundary $\partial\Omega_0$ (in gray). A particle diffuses (blue trajectory) from a starting point $\boldsymbol{x}$ (black filled circle) towards an anisotropic target Γ (in red).

spheroidal targets, for which the trapping length can be computed exactly in any space dimension $d \geqslant 3$. These targets are also used for numerical validation of the proposed approximation.

The paper is organized as follows. In Sec. II, we formulate the general first-passage problem and derive an approximation for the principal eigenvalue λ_1. Section III is devoted to the effect of target anisotropy analyzed for spheroidal domains. In Sec. IV, we discuss the main results and their implications, as well as further perspectives. The Appendixes contain some technical derivations.

II. MAIN RESULTS

We consider a particle that starts from a point $\boldsymbol{x}$ and diffuses with a diffusion coefficient D inside a confining domain $\Omega \subset \mathbb{R}^d$ with a smooth boundary $\partial\Omega = \partial\Omega_0 \cup \Gamma$ composed of two disjoint parts: a reflecting "outer" boundary $\partial\Omega_0$ and a partially reactive "inner" target Γ with a reactivity κ (Fig. 1). Let τ denote the first-reaction time, i.e., the instance when the particle reacts on the target. The survival probability of the particle (i.e., the probability that the particle has not reacted up to time t), $S_q(t|\boldsymbol{x}) = \mathbb{P}_{\boldsymbol{x}}\{\tau > t\}$, satisfies the (backward) diffusion equation

$$\partial_t S_q(t|\boldsymbol{x}) = D\Delta S_q(t|\boldsymbol{x}) \quad (\boldsymbol{x} \in \Omega), \tag{1}$$

subject to the uniform initial condition $S_q(0|\boldsymbol{x}) = 1$ and mixed Robin-Neumann boundary conditions [3]:

$$\begin{aligned}(D\partial_n + \kappa)S_q(t|\boldsymbol{x}) &= 0 \quad (\boldsymbol{x} \in \Gamma),\\ \partial_n S_q(t|\boldsymbol{x}) &= 0 \quad (\boldsymbol{x} \in \partial\Omega_0).\end{aligned} \tag{2}$$

Here Δ is the Laplace operator, ∂_n is the normal derivative oriented away from the domain, and $q = \kappa/D$. The survival probability admits a general spectral decomposition [3,28],

$$S_q(t|\boldsymbol{x}) = \sum_{k=1}^{\infty} e^{-Dt\lambda_k^{(q)}} u_k^{(q)}(\boldsymbol{x}) \int_\Omega d\boldsymbol{x}' \left[u_k^{(q)}(\boldsymbol{x}')\right]^*, \tag{3}$$

where the asterisk denotes the complex conjugate, and $\lambda_k^{(q)}$ and $u_k^{(q)}(\boldsymbol{x})$ are the eigenvalues and orthonormal eigenfunctions of the (negative) Laplace operator in Ω, subject to mixed Robin-Neumann boundary conditions:

$$\Delta u_k^{(q)}(\boldsymbol{x}) + \lambda_k^{(q)} u_k^{(q)}(\boldsymbol{x}) = 0 \quad (\boldsymbol{x} \in \Omega), \tag{4a}$$

$$(\partial_n + q)u_k^{(q)}\big|_\Gamma = 0, \quad \partial_n u_k^{(q)}\big|_{\partial\Omega_0} = 0. \tag{4b}$$

In general, the survival probability that fully characterizes the distribution of the first-reaction time exhibits a sophisticated dependence on the shapes of the domain and of the target, on the location of the starting point $\boldsymbol{x}$, on the diffusive dynamics (here, the diffusivity D), and on the reaction mechanism (here, the reactivity κ). Various aspects of this dependence have been investigated in the past [16,21,25–27,29,43,56–58,89–92].

In this paper, we focus on a common setting when the target is small and located far away from the reflecting boundary $\partial\Omega_0$ of the confining domain Ω. In this section, we will obtain the following approximation to the principal (smallest) eigenvalue $\lambda_1^{(q)}$ of the Laplace operator:

$$\lambda_1^{(q)} \approx \frac{q|\Gamma|}{|\Omega|(1 + qL)}, \tag{5}$$

where

$$L = \frac{|\Gamma|}{C}, \tag{6}$$

which we call the trapping length of the target. Here C is the harmonic (or Newtonian) capacity of the target (see below), $|\Omega|$ is the Lebesgue measure of Ω (e.g., its volume in three dimensions), and $|\Gamma|$ is the Lebesgue measure of the target Γ (e.g., its surface area in three dimensions). In the following, we describe the role of the trapping length L and its relation to the shape of the target. We also check the accuracy of this approximation and discuss immediate applications of this approximation for the decay time, the mean first-reaction time, and the reaction rate.

A. Harmonic capacity

We start by recalling the notion of capacitance, which plays one of the central roles in electrostatics. The capacitance C of an isolated conductor $\mathcal{C}$ in $\mathbb{R}^3$ is the total charge on the conductor's surface when it is maintained at unit potential [93,94]. In mathematical terms, the capacitance can be defined as

$$C = \epsilon_0 \int_{\mathbb{R}^3\backslash\mathcal{C}} d\boldsymbol{x}\, |\nabla\Psi|^2, \tag{7}$$

where $\epsilon_0 \approx 8.854 \times 10^{-12}$ F/m is the vacuum permittivity, and $\Psi(\boldsymbol{x})$ is the (dimensionless) electric potential outside the conductor satisfying

$$\Delta\Psi(\boldsymbol{x}) = 0 \quad (\boldsymbol{x} \in \mathbb{R}^3\backslash\mathcal{C}), \quad \begin{cases}\Psi|_{\partial\mathcal{C}} = 1,\\ \lim_{|\boldsymbol{x}|\to\infty} \Psi(\boldsymbol{x}) = 0.\end{cases} \tag{8}$$

For instance, the capacitance of a ball of radius b is $4\pi\epsilon_0 b$, which follows immediately from the classical radial solution $\Psi(\boldsymbol{x}) = b/|\boldsymbol{x}|$. In the following, we adopt a similar notion of the harmonic (or Newtonian) capacity of a compact set $\mathcal{C}$ in $\mathbb{R}^d$ [95]:

$$C = \int_{\mathbb{R}^d\backslash\mathcal{C}} d\boldsymbol{x}\, |\nabla\Psi|^2, \tag{9}$$

which is identical to Eq. (7) but without the fundamental constant ϵ_0, and $\Psi(\boldsymbol{x})$ satisfies the Laplace equation in $\mathbb{R}^d\backslash\mathcal{C}$. In particular, the capacity of a ball of radius b is $(d-2)\sigma_d b^{d-2}$, where

$$\sigma_d = \frac{2\pi^{d/2}}{\Gamma(d/2)} \tag{10}$$

is the area of the d-dimensional unit ball, with $\Gamma(z)$ being the Euler gamma function (not to be confused with our notation Γ for the target). Note that some authors rescale the capacity as $\hat{C} = \frac{1}{(d-2)\sigma_d} C$ to make the capacity of a ball b^{d-2}.

According to Eq. (8), $\Psi(\boldsymbol{x})$ can also be interpreted as the probability of capture on the perfect target $\Gamma = \partial\mathcal{C}$ of a Brownian particle started from $\boldsymbol{x}$. The perfect target refers to the Dirichlet boundary condition (i.e., $q = \infty$) when the particle is captured by (or adsorbed on, or reacted on, or killed on) the target Γ upon their first encounter. In turn, $1 - \Psi(\boldsymbol{x})$ is the steady-state survival (or escape) probability of that particle [i.e., it is equal to the long-time limit of $S_\infty(t|\boldsymbol{x})$ in the case when there is no outer boundary $\partial\Omega_0$]. Using the Green's formula, one can rewrite Eq. (9) as

$$C = \int_\Gamma d\boldsymbol{x}\, \partial_n \Psi. \tag{11}$$

As a consequence, if there are many independent particles and their concentration is maintained at n_0 at infinity, then $J_\infty = CDn_0$ is the total steady-state diffusive flux onto the perfectly absorbing target Γ, while $K_\infty = J_\infty/n_0 = CD$ is the trapping constant of that target [66]. The analogy between electrostatics and diffusion-controlled reactions has been thoroughly employed in the past [3]. We emphasize that the capacity, which is obtained by solving the Laplace equation in the space outside the target, is the intrinsic property of that target. In other words, there is no outer reflecting boundary here.

B. Approximation for a perfect target

We explore yet another application of the capacity as a leading-term approximation of the smallest eigenvalue $\lambda_1^{(\infty)}$ of the Laplace operator in the presence of a perfect target ($q = \infty$) for which the Robin boundary condition in Eq. (4b) is reduced to the Dirichlet boundary condition $(u_k^{(\infty)})_{|\Gamma} = 0$. This role of the capacity was recognized already by Samarskii in 1948 [96], but more elaborate asymptotic analysis of the Dirichlet Laplace operator eigenvalues was developed in [30,31,40]. Here the target Γ is enclosed by an outer reflecting surface $\partial\Omega_0$ so that the confining domain Ω is bounded (Fig. 1). We assume that the target is small as compared to the confining domain Ω, and it is located far away from the outer reflecting boundary $\partial\Omega_0$, i.e.,

$$\mathrm{diam}\{\Gamma\} \ll |\partial\Omega_0 - \Gamma| \leqslant \mathrm{diam}\{\Omega\}, \tag{12}$$

where $|\partial\Omega_0 - \Gamma|$ is the distance between sets $\partial\Omega_0$ and Γ, and $\mathrm{diam}\{A\} = \sup_{\boldsymbol{x}_1,\boldsymbol{x}_2\in A}\{|\boldsymbol{x}_1 - \boldsymbol{x}_2|\}$ denotes the diameter of a set A. Since mathematical works [31,40] were focused on the three-dimensional setting (as well as the two-dimensional case in [31]), we briefly describe the general arguments valid for any $d \geqslant 3$ (see the discussion for planar domains in Sec. IV).

Integrating Eq. (4a) over $\boldsymbol{x} \in \Omega$ and using the Green's formula, one gets

$$\lambda_1^{(\infty)} = -\frac{\int_\Gamma d\boldsymbol{x}\, \partial_n u_1^{(\infty)}(\boldsymbol{x})}{\int_\Omega d\boldsymbol{x}\, u_1^{(\infty)}(\boldsymbol{x})} \tag{13}$$

(see, e.g., the review [97] for other properties of Laplacian eigenvalues and eigenfunctions). As Γ is small, the numerator is small and thus the principal eigenvalue $\lambda_1^{(\infty)}$ is close to 0. The associated eigenfunction is therefore close to a constant function, $u_1^{(\infty)}(\boldsymbol{x}) \approx u_0$, except for a boundary layer near the target; in particular, the Neumann boundary condition at the outer reflecting boundary can be replaced by the Dirichlet condition $(u_1^{(\infty)})_{|\partial\Omega_0} \approx u_0$. In turn, the eigenfunction $u_1^{(\infty)}(\boldsymbol{x})$ vanishes on the target. One can thus approximate $u_1^{(\infty)}(\boldsymbol{x})$ near the target by setting $u_1^{(\infty)}(\boldsymbol{x}) \approx u_0 v(\boldsymbol{x})$, where $v(\boldsymbol{x})$ is the harmonic function satisfying Dirichlet boundary conditions $v|_\Gamma = 0$ and $v|_{\partial\Omega_0} = 1$. Substituting these approximations into Eq. (13), one gets

$$\lambda_1^{(\infty)} \approx -\frac{\int_\Gamma d\boldsymbol{x}\, \partial_n v(\boldsymbol{x})}{\int_\Omega d\boldsymbol{x}\, v(\boldsymbol{x})}.$$

In the numerator, the integral is carried over the target Γ so that the function $v(\boldsymbol{x})$ can be replaced by its limit $1 - \Psi(\boldsymbol{x})$, which is obtained by moving the outer boundary $\partial\Omega_0$ to infinity. In other words, a distant outer boundary $\partial\Omega_0$ does not have much of an influence on the solution in the vicinity of the target. In turn, the denominator is the integral over the domain Ω, in which $v(\boldsymbol{x})$ is nearly constant, except for a vicinity of the small target. Therefore, we replace $v(\boldsymbol{x})$ by 1 here. Upon these two approximations, one gets

$$\lambda_1^{(\infty)} \approx \frac{\int_\Gamma d\boldsymbol{x}\, \partial_n \Psi(\boldsymbol{x})}{|\Omega|} = \frac{C}{|\Omega|}. \tag{14}$$

Figure 2 illustrates the behavior of the eigenfunction $u_1^{(\infty)}(\boldsymbol{x})$ and its approximation by $v(\boldsymbol{x})$ for a shell-like domain between two concentric spheres, for which these two functions are known explicitly.

Moreover, Maz'ya *et al.* as well as Cheviakov and Ward provided the next-order correction to this approximation in three dimensions [31,40]. In our setting of a single target, their result reads

$$\lambda_1^{(\infty)} \approx \frac{C'}{|\Omega|}, \tag{15}$$

where C' can be understood as a "corrected" capacity:

$$C' = C - C^2 R_N(\boldsymbol{x}_\Gamma, \boldsymbol{x}_\Gamma). \tag{16}$$

Here $R_N(\boldsymbol{x}, \boldsymbol{x}')$ is the regular part of the Neumann Green's function, and $\boldsymbol{x}_\Gamma$ is the location of (the center of) the target Γ. The Neumann Green's function is defined in the confining domain *without any target* as

$$\Delta G_N(\boldsymbol{x}, \boldsymbol{x}') = \frac{1}{|\Omega|} - \delta(\boldsymbol{x} - \boldsymbol{x}') \quad (\boldsymbol{x} \in \Omega), \tag{17a}$$

$$\partial_n(G_N)|_{\partial\Omega_0} = 0, \qquad \int_\Omega d\boldsymbol{x}\, G_N(\boldsymbol{x}, \boldsymbol{x}') = 0, \tag{17b}$$

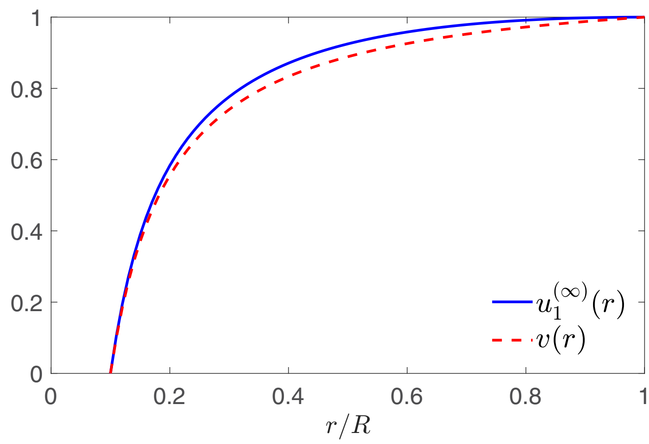

FIG. 2. The eigenfunction $u_1^{(\infty)}(r)$ of the Laplace operator in a three-dimensional shell-like domain between two concentric spheres of radii $b = 0.1$ and $R = 1$, with the Dirichlet boundary condition on the target, $u_1^{(\infty)}(b) = 0$, and the Neumann boundary condition on the outer sphere, $(\partial_r u_1^{(\infty)})(R) = 0$. This eigenfunction is known explicitly (see [29] for details) and depends only on the radial coordinate $r = |\boldsymbol{x}|$. For comparison, the harmonic function $v(r) = (1/b - 1/r)/(1/b - 1/R)$ satisfying $v(b) = 0$ and $v(R) = 1$ is shown by a dashed line.

and its regular part is

$$G_N(\boldsymbol{x}, \boldsymbol{x}') = \frac{1}{4\pi|\boldsymbol{x} - \boldsymbol{x}'|} + R_N(\boldsymbol{x}, \boldsymbol{x}'). \tag{18}$$

In other words, both $G_N(\boldsymbol{x}, \boldsymbol{x}')$ and $R_N(\boldsymbol{x}, \boldsymbol{x}')$ depend only on the confining domain but are independent of the target. For a spherical domain of radius R, Cheviakov and Ward derived an explicit expression for the Neumann Green's function and its regular part [40]. In particular, they found

$$R\, R_N(\boldsymbol{x}, \boldsymbol{x}) = \frac{1}{4\pi(1 - |\boldsymbol{x}|^2/R^2)} - \frac{1}{4\pi}\ln(1 - |\boldsymbol{x}|^2/R^2) + \frac{|\boldsymbol{x}|^2}{4\pi R^2} - \frac{7}{10\pi}. \tag{19}$$

For instance, if the target is located at the center, one has $R_N(\boldsymbol{0}, \boldsymbol{0}) = -9/(20\pi R)$. We will discuss the accuracy of this approximation in Sec. III.

C. Global mean first-reaction time

The next step consists in extending the above approximation to a partially reactive target. For this purpose, we employ the relation between the smallest eigenvalue $\lambda_1^{(q)}$ and the so-called global mean first-reaction time, T_q, which is defined as the volume average of the mean first-reaction time $T_q(\boldsymbol{x}) = \langle\tau\rangle$:

$$T_q = \frac{1}{|\Omega|}\int_\Omega d\boldsymbol{x}\, T_q(\boldsymbol{x}). \tag{20}$$

In other words, the starting point is considered here as being uniformly distributed inside the confining domain. In turn, $T_q(\boldsymbol{x})$ satisfies the boundary value problem [3]

$$D\Delta T_q(\boldsymbol{x}) = -1 \quad (\boldsymbol{x} \in \Omega), \tag{21a}$$

$$(\partial_n + q)T_q(\boldsymbol{x}) = 0 \quad (\boldsymbol{x} \in \Gamma), \tag{21b}$$

$$\partial_n T_q(\boldsymbol{x}) = 0 \quad (\boldsymbol{x} \in \partial\Omega_0). \tag{21c}$$

The integral of Eq. (21a) over $\boldsymbol{x} \in \Omega$ implies

$$-|\Omega| = \int_\Omega d\boldsymbol{x}\, D\Delta T_q(\boldsymbol{x}) = \int_\Gamma d\boldsymbol{x}\, D(\partial_n T_q(\boldsymbol{x})) = -\kappa \int_\Gamma d\boldsymbol{x}\, T_q(\boldsymbol{x}),$$

i.e.,

$$\int_\Gamma d\boldsymbol{x}\, T_q(\boldsymbol{x}) = \frac{|\Omega|}{\kappa}. \tag{22}$$

Curiously, this integral does not depend on the diffusion coefficient D.

To proceed, we multiply Eq. (21a) by $T_\infty(\boldsymbol{x})$, subtract from it Eq. (21a) with $q = \infty$ multiplied by $T_q(\boldsymbol{x})$, and integrate over $\boldsymbol{x} \in \Omega$:

$$\begin{aligned}(T_q - T_\infty)|\Omega| &= \int_\Omega d\boldsymbol{x}(T_q(\boldsymbol{x}) - T_\infty(\boldsymbol{x}))\\ &= \int_\Omega d\boldsymbol{x}(T_\infty(\boldsymbol{x})\, D\Delta T_q(\boldsymbol{x}) - T_q(\boldsymbol{x})\, D\Delta T_\infty(\boldsymbol{x}))\\ &= \int_\Gamma d\boldsymbol{x}(\underbrace{T_\infty(\boldsymbol{x})}_{=0}\, D\partial_n T_q(\boldsymbol{x}) - T_q(\boldsymbol{x})\, D\partial_n T_\infty(\boldsymbol{x})).\end{aligned}$$

Note that $T_\infty(\boldsymbol{x})$ can be obtained by integrating the Dirichlet-Neumann Green's function, $G(\boldsymbol{x}|\boldsymbol{x}_0)$, satisfying

$$-D\Delta G(\boldsymbol{x}|\boldsymbol{x}_0) = \delta(\boldsymbol{x} - \boldsymbol{x}_0) \quad (\boldsymbol{x} \in \Omega), \tag{23a}$$

$$G(\boldsymbol{x}|\boldsymbol{x}_0) = 0 \quad (\boldsymbol{x} \in \Gamma), \tag{23b}$$

$$\partial_n G(\boldsymbol{x}|\boldsymbol{x}_0) = 0 \quad (\boldsymbol{x} \in \partial\Omega_0), \tag{23c}$$

as follows:

$$T_\infty(\boldsymbol{x}) = \int_\Omega d\boldsymbol{x}_0\, G(\boldsymbol{x}|\boldsymbol{x}_0). \tag{24}$$

As a consequence, $-D\partial_n T_\infty(\boldsymbol{x})$ turns out to be proportional to the harmonic measure density [98], $\omega(\boldsymbol{x}|\boldsymbol{x}_0)$, averaged over $\boldsymbol{x}_0$:

$$\omega(\boldsymbol{x}) \equiv \frac{1}{|\Omega|}\int_\Omega d\boldsymbol{x}_0\, \omega(\boldsymbol{x}|\boldsymbol{x}_0) = \frac{1}{|\Omega|}\int_\Omega d\boldsymbol{x}_0\, (-D\partial_n G(\boldsymbol{x}|\boldsymbol{x}_0)) = -\frac{1}{|\Omega|} D\partial_n T_\infty(\boldsymbol{x}). \tag{25}$$

We conclude that

$$T_q = T_\infty + \int_\Gamma d\boldsymbol{x}\, \omega(\boldsymbol{x})\, T_q(\boldsymbol{x}). \tag{26}$$

This relation that we formally obtained from the boundary value problem (21) has a clear probabilistic interpretation. In fact, the first-reaction time τ can be naturally split into two contributions, $\tau = \tau_\infty + \tau_\Gamma$, where τ_∞ is the first-passage time to the target (i.e., the instance of the first arrival onto the target), and τ_Γ is the first-reaction time for a particle that was started on the target Γ. Accordingly, T_∞ is the volume-averaged mean value of τ_∞, whereas the second term in Eq. (26) is the target-surface-averaged mean value of τ_Γ. Indeed, $\omega(\boldsymbol{x})$ describes the probability density of the first arrival in the vicinity of a boundary point $\boldsymbol{x} \in \Gamma$, from which the particle continues to diffuse until the reaction on Γ. In other words, the second term is the average of $T_q(\boldsymbol{x})$ over the random first arrival point on Γ. Qualitatively, the first and second terms represent, respectively, diffusion-limited and reaction-limited contributions. As is expected, the first term depends on the diffusion coefficient D but is independent of the reactivity κ. In contrast, the second term formally depends on both D and κ. However, when the target is small, the volume-averaged harmonic measure density $\omega(\boldsymbol{x})$ is expected to be almost uniform:

$$\omega(\boldsymbol{x}) \approx \frac{1}{|\Gamma|}. \tag{27}$$

Substituting this approximation into Eq. (26) and using Eq. (22), we deduce

$$T_q \approx T_\infty + \frac{|\Omega|}{\kappa|\Gamma|}. \tag{28}$$

In this approximation, the second term depends only on the reactivity κ but is independent of the diffusion coefficient D. The relation (28) represents, therefore, two consecutive additive contributions to the global mean first-reaction time: the diffusion-limited contribution T_∞ describing the transport of the particle towards the target, and the reaction-limited contribution due to the partial reactivity of the target. These two complementary contributions to the mean first-reaction time were discussed earlier for some symmetric domains [29,54]. However, we are not aware of earlier derivations of this representation in the general setting. A similar separation of diffusion-limited and reaction-limited contributions to the steady-state diffusive flux J_q can be already identified in the Collins-Kimball solution for a spherical target of radius b in $\mathbb{R}^3$ [11] (see also [63,99]):

$$\frac{4\pi b^2 n_0}{J_q} = \frac{b}{D} + \frac{1}{\kappa}. \tag{29}$$

In the same vein, two contributions to the impedance of a partially blocking electrode have been identified and discussed [74,75,78,81].

D. Partially reactive target

To complete our derivation, we evaluate the global mean first-reaction time T_q according to its definition

$$T_q = \int_0^\infty dt\, t\,(-\partial_t S_q(t)) = \int_0^\infty dt\, S_q(t), \tag{30}$$

where $-\partial_t S_q(t)$ is the probability density of the first-reaction time (averaged over the starting point), with

$$S_q(t) = \frac{1}{|\Omega|}\int_\Omega d\boldsymbol{x}\, S_q(t|\boldsymbol{x}) = \sum_{k=1}^\infty c_k^{(q)}\, e^{-Dt\lambda_k^{(q)}}, \tag{31}$$

where

$$c_k^{(q)} = \frac{1}{|\Omega|}\left|\int_\Omega d\boldsymbol{x}\, u_k^{(q)}(\boldsymbol{x})\right|^2, \tag{32}$$

and we used the spectral expansion (3). Since $S_q(0) = 1$, the positive coefficients $c_k^{(q)}$ can be understood as the relative weights of the Laplacian eigenfunctions $u_k^{(q)}(\boldsymbol{x})$ in the survival probability $S_q(t)$.

When the target is small, the ground eigenfunction $u_1^{(q)}(\boldsymbol{x})$ is almost constant in Ω (except for a layer near the target; see above). As a consequence, other eigenfunctions, which are orthogonal to $u_1^{(q)}$, have small contributions to $S_q(t)$, with $c_k^{(q)} \approx 0$ for $k > 1$, whereas $c_1^{(q)} \approx 1$ (see further discussion in [100,101]). In other words,

$$S_q(t) \approx e^{-Dt\lambda_1^{(q)}}, \tag{33}$$

which implies, according to Eq. (30), the following approximation:

$$T_q \approx \frac{1}{D\lambda_1^{(q)}}. \tag{34}$$

Substituting Eq. (28) into this relation, we finally arrive at

$$\lambda_1^{(q)} \approx \frac{1}{D\big(T_\infty + \frac{|\Omega|}{\kappa|\Gamma|}\big)} \approx \frac{1}{\frac{1}{\lambda_1^{(\infty)}} + \frac{|\Omega|}{q|\Gamma|}} \approx \frac{1}{\frac{|\Omega|}{C} + \frac{|\Omega|}{q|\Gamma|}},$$

which implies the expression (5). This relation can also be expressed in terms of the global mean first-reaction time from Eq. (34):

$$T_q \approx \frac{|\Omega|}{|\Gamma|}\left(\frac{L}{D} + \frac{1}{\kappa}\right), \tag{35}$$

which represent the sum of diffusion-limited and reaction-limited contributions. Accordingly, $1/T_q$ can be interpreted as the overall reaction rate, while T_q is also the decay time of the survival probability at long times, $S_q(t|\boldsymbol{x}) \propto e^{-Dt\lambda_1^{(q)}}$; see Eq. (3). Note that this asymptotic relation was employed to compute the principal eigenvalue numerically via estimating the survival probability [102].

Moreover, the principal eigenvalue $\lambda_1^{(q)}$ can be used to determine the steady-state diffusive flux and the trapping constant of a small target. In fact, the probability density $H_q(t|\boldsymbol{x})$ of the first-reaction time can also be understood as the probability flux onto the target from a fixed point $\boldsymbol{x}$. At long times, the spectral expansion (3) implies

$$H_q(t|\boldsymbol{x}) \approx D\lambda_1^{(q)}\, e^{-D\lambda_1^{(q)}t}\, u_1^{(q)}(\boldsymbol{x}) \int_\Omega d\boldsymbol{x}'\, u_1^{(q)}(\boldsymbol{x}'). \tag{36}$$

As in Sec. II B, one can argue that $u_1^{(q)}(\boldsymbol{x})$ is nearly constant for any $\boldsymbol{x}$ far from the target so that

$$H_q(t|\boldsymbol{x}) \approx D\lambda_1^{(q)}\, e^{-D\lambda_1^{(q)}t}, \tag{37}$$

where we used the $L_2(\Omega)$ normalization of $u_1^{(q)}(\boldsymbol{x})$. If there are many independent particles with a concentration n_0, their total diffusive flux onto the target is $J_q(t) \approx n_0|\Omega|H_q(t|\boldsymbol{x})$. Expectedly, this flux vanishes in the long-time limit because all particles that were initially present in a bounded domain react on the target. However, if the target is very small, there is an intermediate range of times for which Eq. (37) holds but $D\lambda_1^{(q)}t \ll 1$, so that

$$J_q \approx n_0|\Omega|D\lambda_1^{(q)} \approx n_0 D\frac{q|\Gamma|}{1+qL}, \tag{38}$$

where we used our approximation (5) for $\lambda_1^{(q)}$. This is an extension of the Collins-Kimball relation (29) that was derived for a spherical target. While we derived the approximate relation (38) by considering the limit of very small targets, one could alternatively fix the target size and move the outer boundary $\partial\Omega_0$ to infinity. In other words, this relation is applicable to a bounded target of any size in $\mathbb{R}^d$ (i.e., without $\partial\Omega_0$). Dividing the total flux by n_0 yields the trapping constant:

$$K_q \approx D\frac{q|\Gamma|}{1+qL}. \tag{39}$$

In the limit $q \to \infty$, we retrieve the known approximations $J_\infty \approx n_0 DC$ and $K_\infty \approx CD$ for perfectly reactive targets that we mentioned in Sec. II A.

In summary, the approximate relation (5) relies on three approximations, (14), (28), and (33), which are all based on the assumption of the target smallness. We stress that we do not claim the above derivation is mathematically rigorous. A more rigorous derivation of Eq. (5) presents an interesting perspective.

III. TARGET ANISOTROPY

In former works on partially reactive targets [11,13,44,46,50,52–54,67,72–88], the reaction length $1/q = D/\kappa$ was generally compared to a "typical size" of the target, without providing its definition. For a spherical (or, more generally, "roundish") target, there is a single geometric lengthscale, its diameter (or radius), which is naturally compared with $1/q$. In turn, when the target has an approximately isotropic shape but a rough boundary, other geometric lengthscales can emerge. For instance, in the study of steady-state diffusion of oxygen molecules towards the acinar surface in the lungs, Sapoval *et al.* introduced the relevant lengthscale $L_S = |\Gamma|/\mathrm{diam}\{\Gamma\}$ as the surface area of the target divided by its diameter [77]. As the surface area of a compact target with a rough (e.g., fractal-like) boundary can be extremely large, the length L_S can be orders of magnitude larger than the diameter itself.

The explicit approximation (5) allows us to identify the relevant lengthscale of a small target in a more general setting and beyond the steady-state regime. The trapping length $L = |\Gamma|/C$ generalizes the above length L_S to anisotropic targets and in higher dimensions. These two lengths are comparable for a nearly isotropic target in three dimensions because the capacity of such a target is comparable to its diameter. In this section, we investigate how the target anisotropy affects the trapping length L and therefore various properties of diffusion-reaction processes.

A. Prolate spheroids

We model an elongated target by the surface of a d-dimensional prolate spheroid (i.e., an ellipsoid of revolution) with the single major semiaxis b along the dth coordinate, and equal minor semiaxes $a < b$:

$$\Gamma_{a,b} = \left\{(x_1,\dots,x_d)\in\mathbb{R}^d : \frac{x_1^2}{a^2}+\dots+\frac{x_{d-1}^2}{a^2}+\frac{x_d^2}{b^2}=1\right\}. \tag{40}$$

The capacity of a prolate spheroid in three dimensions is well known [94]:

$$C_{a,b}^{(3)} = \frac{8\pi c}{\ln\left(\frac{1+c/b}{1-c/b}\right)}, \tag{41}$$

where $c = \sqrt{b^2-a^2}$. In the limit $a \to b$, this relation is reduced to the classical capacity of a ball of radius b: $C_{b,b}^{(3)} = 4\pi b$. An extension of this result to higher dimensions was discussed in [103]. In Appendix A, we describe this extension and obtain the following compact expression:

$$C_{a,b}^{(d)} = \frac{(d-2)\sigma_d\, b\, a^{d-3}}{{}_2F_1\left(\frac{1}{2},1;\frac{d}{2};1-\frac{a^2}{b^2}\right)}, \tag{42}$$

where ${}_2F_1(a,b;c;z)$ is the hypergeometric function, and σ_d is given by Eq. (10). For even dimensions, one gets particularly simple expressions, e.g.,

$$C_{a,b}^{(4)} = 2\pi^2 a(a+b), \tag{43a}$$

$$C_{a,b}^{(6)} = \frac{3\pi^3 a^3(a+b)^2}{2a+b}. \tag{43b}$$

In the limit $a \to b$, one retrieves the capacity of the ball: $C_{b,b}^{(d)} = (d-2)\sigma_d b^{d-2}$. In turn, in the opposite limit of highly anisotropic targets, $a \to 0$, one can use Euler's identity to get in the leading order

$$C_{a,b}^{(d)} \approx (d-3)\sigma_d\, b\, a^{d-3} \quad (d>3). \tag{44}$$

For $d = 3$, Eq. (41) yields

$$C_{a,b}^{(3)} \approx \frac{4\pi b}{\ln(b/a)}, \tag{45}$$

i.e., the capacity vanishes very slowly. When the target is surrounded by a concentric spherical surface $\partial\Omega_0$ of radius R, the volume of the confining domain is

$$|\Omega| = \frac{\pi^{d/2}}{\Gamma(d/2+1)}(R^d - ba^{d-1}). \tag{46}$$

Figure 3(a) illustrates the behavior of the principal eigenvalue $\lambda_1^{(\infty)}$ for a perfectly reactive target ($q = \infty$). On this log-log plot, one sees the expected power-law dependence on the minor semiaxis a. Our approximation (14) is least accurate in three dimensions (thin blue curve) and gets more and more accurate as the space dimension d increases. Note that the use of the "corrected" capacity C' in Eq. (16) instead of C significantly improves the accuracy of the approximation in three dimensions (thick blue curve). In Fig. 3(c), filled symbols show the relative error of the approximation (14) for $d > 3$ and of Eq. (15) for $d = 3$. For the considered major semiaxis $b = 0.2$, the relative error does not exceed 10%.

The surface area of prolate spheroids is also discussed in Appendix A:

$$\left|\Gamma_{a,b}^{(d)}\right| = \sigma_d\, a^{d-2}\, b\, {}_2F_1\left(\frac{1}{2},-\frac{1}{2};\frac{d}{2};1-\frac{a^2}{b^2}\right). \tag{47}$$

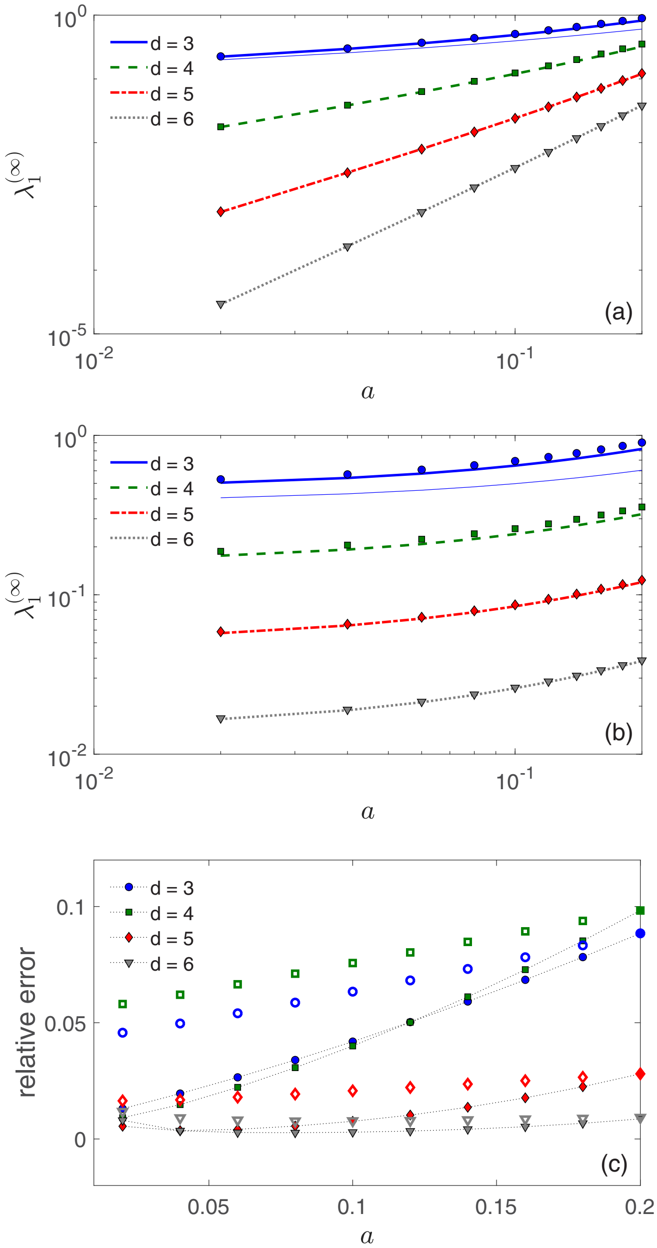

FIG. 3. (a), (b) The principal eigenvalue $\lambda_1^{(\infty)}$ of the Laplace operator for a perfectly reactive prolate (a) and oblate (b) spheroidal target with semiaxes $a \leqslant b = 0.2$ surrounded by a concentric reflecting spherical surface of radius $R = 1$. Symbols present the numerical computation by a finite-elements method (see Appendix D), whereas thick lines show the approximate relation (14). In three dimensions, a thick blue line presents the improved approximation (15) with the "corrected" capacity C' from Eq. (16), whereas a thin blue line indicates the leading-order approximation (14). (c) The relative error of the above approximations shown by filled symbols for prolate spheroids and by empty symbols for oblate spheroids in $\mathbb{R}^d$ with $d = 3, 4, 5, 6$ (see the legend). Note that a minor increase of the relative error for $d = 6$ at small a can be a numerical artifact due to an insufficient mesh size.

As $a \to 0$, one gets in the lowest order

$$\left|\Gamma_{a,b}^{(d)}\right| \approx 2\pi^{d/2} a^{d-2} b \,\frac{\Gamma(d/2)}{\Gamma\left(\frac{d-1}{2}\right)\Gamma\left(\frac{d+1}{2}\right)}. \tag{48}$$

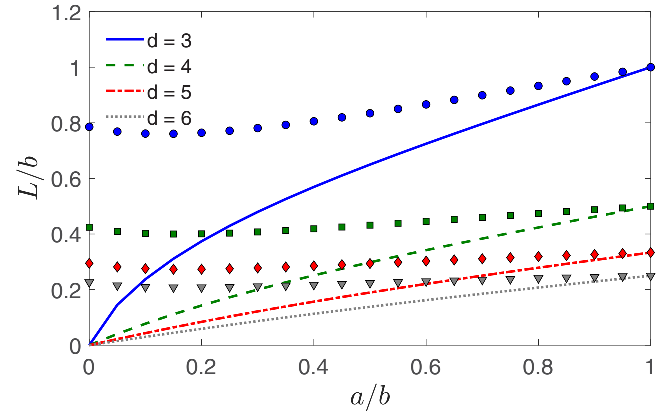

FIG. 4. The trapping length L from Eqs. (49) and (59) of prolate (lines) and oblate (symbols) spheroids for several dimensions d. Note that $L/b = 1/(d-2)$ at $a/b = 1$.

Substituting Eqs. (42) and (47) into Eq. (6), we get the trapping length

$$L = \frac{a}{d-2}\, {}_2F_1\left(\frac{1}{2}, -\frac{1}{2}; \frac{d}{2}; 1 - \frac{a^2}{b^2}\right) {}_2F_1\left(\frac{1}{2}, 1; \frac{d}{2}; 1 - \frac{a^2}{b^2}\right). \tag{49}$$

For a spherical target ($a = b$), one retrieves $L = b/(d-2)$. In the opposite limit $a \to 0$ of highly anisotropic targets, we obtain

$$L \approx a\,\frac{\Gamma^2\left(\frac{d}{2}\right)}{(d-3)\Gamma\left(\frac{d-1}{2}\right)\Gamma\left(\frac{d+1}{2}\right)} \quad (d > 3), \tag{50a}$$

$$L \approx \frac{\pi}{4}\, a \ln(b/a) \quad (d = 3). \tag{50b}$$

In both cases, the lengthscale L vanishes, and the trapping capacity of a very thin target becomes essentially reaction-limited for any finite reactivity: $\lambda_1^{(q)} \approx q|\Gamma|/|\Omega|$.

The dependence (49) of the trapping length L on the aspect ratio a/b is shown by lines in Fig. 4. A linear scaling of L with a is observed in all dimensions $d > 3$, whereas the curve for $d = 3$ exhibits a linear scaling with a logarithmic correction.

Figure 5(a) shows the principal eigenvalue $\lambda_1^{(q)}$ as a function of q for a prolate spheroid of a fixed aspect ratio $a/b = 0.5$. One sees that our approximation (5) is very accurate over a broad range of q values and all dimensions $d \geqslant 3$.

B. Oblate spheroids

A flattened target is modeled by the surface of a d-dimensional oblate spheroid with the single minor semiaxis a along the dth coordinate, and equal major semiaxes $b > a$:

$$\tilde{\Gamma}_{a,b} = \left\{(x_1, \ldots, x_d) \in \mathbb{R}^d : \frac{x_1^2}{b^2} + \cdots + \frac{x_{d-1}^2}{b^2} + \frac{x_d^2}{a^2} = 1\right\}. \tag{51}$$

The capacity of an oblate spheroid in three dimensions is well known [94]:

$$\tilde{C}_{a,b}^{(3)} = \frac{4\pi c}{\cos^{-1}(a/b)}. \tag{52}$$

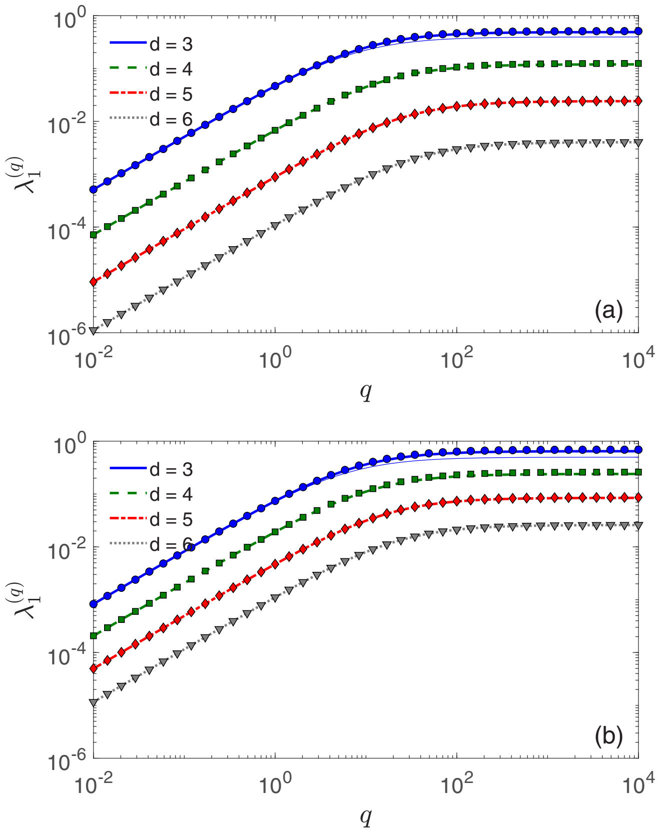

FIG. 5. The principal eigenvalue $\lambda_1^{(q)}$ as a function q for prolate (a) and oblate (b) spheroidal targets with semiaxes $a = 0.1$ and $b = 0.2$ surrounded by a reflecting concentric spherical surface of radius $R = 1$. Symbols present the numerical computation by a finite-elements method (see Appendix D), whereas thick lines show the approximate relation (5). In three dimensions, a thick blue line presents Eq. (5) with the "corrected" capacity C' from Eq. (16), whereas a thin blue line corresponds to the capacity C. The trapping length L given by Eqs. (49) and (59) is 0.1300, 0.0596, 0.0379, and 0.0276 for prolate spheroids, and 0.1669, 0.0864, 0.0588, and 0.0447 for oblate spheroids, with $d = 3, 4, 5, 6$, respectively.

In the limit $a \to b$, one retrieves the capacity of the ball of radius b; in the opposite limit $a \to 0$, this relation yields the well-known result for the capacity of the disk of radius b: $\tilde{C}_{0,b}^{(3)} = 8\cancel{\pi}b$.

In Appendix B, we recall the derivation of the capacity in higher dimensions and derive the following compact expression:

$$\tilde{C}_{a,b}^{(d)} = \frac{(d-2)\sigma_d\, b^{d-2}}{{}_2F_1\left(\frac{1}{2}, \frac{d-2}{2}; \frac{d}{2}; 1 - a^2/b^2\right)}. \tag{53}$$

For even dimensions, one gets particularly simple relations, e.g.,

$$\tilde{C}_{a,b}^{(4)} = 2\pi^2 b(a+b), \tag{54a}$$

$$\tilde{C}_{a,b}^{(6)} = \frac{3\pi^3 b^3 (a+b)^2}{2b+a}. \tag{54b}$$

As $a \to 0$, the capacity reaches a finite limit:

$$\tilde{C}_{0,b}^{(d)} = \frac{(d-2)\sigma_d\, b^{d-2}\Gamma\left(\frac{d-1}{2}\right)}{\Gamma\left(\frac{d}{2}\right)\sqrt{\pi}}. \tag{55}$$

In contrast to the case of infinitely thin elongated targets [cf. Eq. (44)], flattened targets remain accessible to Brownian motion. When the target is surrounded by a concentric spherical surface $\partial\Omega_0$ of radius R, the volume of the confining domain is

$$|\tilde{\Omega}| = \frac{\pi^{d/2}}{\Gamma(d/2+1)}(R^d - ab^{d-1}). \tag{56}$$

The accuracy of the approximation (5) for perfectly reactive oblate targets is illustrated in Fig. 3(b). As for elongated targets, the approximation is least accurate for $d = 3$ and gets more and more accurate as d increases. Its relative error is shown in Fig. 3(c) by empty symbols.

The surface area of oblate spheroids is discussed in Appendix B:

$$\left|\tilde{\Gamma}_{a,b}^{(d)}\right| = \sigma_d\, b^{d-1}\, {}_2F_1\left(\frac{d-1}{2}, -\frac{1}{2}; \frac{d}{2}; 1 - \frac{a^2}{b^2}\right). \tag{57}$$

In the limit $a \to 0$, one gets

$$\left|\tilde{\Gamma}_{0,b}^{(d)}\right| = b^{d-1}\frac{2\pi^{(d-1)/2}}{\Gamma\left(\frac{d+1}{2}\right)}. \tag{58}$$

For instance, one retrieves the surface area of a two-sided disk for $d = 3$: $|\tilde{\Gamma}_{0,b}^{(3)}| = 2\pi b^2$ (it is twice as big as the area of the disk because there are two faces).

Substituting Eqs. (53) and (57) into Eq. (6), we get the trapping length:

$$L = \frac{b}{d-2}\, {}_2F_1\left(\frac{d-1}{2}, -\frac{1}{2}; \frac{d}{2}; 1 - \frac{a^2}{b^2}\right) \times {}_2F_1\left(\frac{1}{2}, \frac{d-2}{2}; \frac{d}{2}; 1 - \frac{a^2}{b^2}\right). \tag{59}$$

In contrast to the case of prolate spheroids, the trapping length here remains of the order of b for any a, ranging from

$$L = \frac{b}{d-2}\frac{\Gamma^2\left(\frac{d}{2}\right)}{\Gamma\left(\frac{d-1}{2}\right)\Gamma\left(\frac{d+1}{2}\right)} \quad (a = 0) \tag{60}$$

to $L = b/(d-2)$ at $a = b$. This behavior is shown in Fig. 4 by symbols. Curiously, the dependence is not monotonous, but variations of L with a/b are insignificant, particularly at larger d. We conclude that flattening the target does not almost change its trapping capacity. The accuracy of the approximation (5) for a partially reactive oblate target is illustrated in Fig. 5(b).

IV. DISCUSSION AND CONCLUSION

In this paper, we investigated restricted diffusion inside a bounded domain towards a partially reactive target. Our first result is a simple explicit approximation (5) for the principal eigenvalue of the Laplace operator with mixed Robin-Neumann boundary conditions. This approximation involves very basic geometric characteristics such as the volume of the confining domain $|\Omega|$, the surface area of the target $|\Gamma|$, and its harmonic capacity C. The dependence on the physical transport parameters — the diffusion coefficient D and the reactivity κ — is fully explicit. Even though the derivation of Eq. (5) involved three approximations, all of them were based on the smallness of the target and its distant location from the reflecting boundary. A comparison with a numerical solution by a finite-elements method showed that the approximation is getting more and more accurate as the space dimension increases. In three dimensions, the use of the "corrected" capacity C' allows one to get accurate results as well. As the principal eigenvalue $\lambda_1^{(q)}$ determines several characteristics of diffusion-controlled reactions, the proposed approximation opens access to them in a simple way.

The second result is the identification of the relevant geometric lengthscale of the target that we called the trapping length: $L = |\Gamma|/C$. This length naturally emerges from our approximation as the geometric scale, to which the physical reaction length $1/q = D/\kappa$ has to be compared. This trapping length generalizes a former length $L_S = |\Gamma|/\mathrm{diam}\{\Gamma\}$, introduced by Sapoval *et al.* [77], to anisotropic targets and higher dimensions. The simple form of the trapping length is quite intuitive. In fact, the surface area $|\Gamma|$ naturally appears in the reaction-limited regime ($q \to 0$) when the transport step is fast as compared to the reaction step, and thus the reaction event occurs on any target point with almost equal probabilities (i.e., the so-called spread harmonic measure is almost uniform; see [88,104]). For instance, the principal eigenvalue exhibits the well-known behavior $\lambda_1^{(q)} \approx q|\Gamma|/|\Omega|$. In the opposite diffusion-limited regime ($q \to \infty$), the trapping capacity of the target is determined by its capacity C, yielding $\lambda_1^{(q)} \approx C/|\Omega|$. The role of the capacity as the principal geometric characteristic of the target can be recognized in the seminal paper by Smoluchowski [105], in which the steady-state flux was shown to be proportional to the radius of a spherical target, i.e., to its capacity. While the reaction length $1/q = D/\kappa$ is the ratio of two transport coefficients, the trapping length $L = |\Gamma|/C$ is the ratio of the associated geometric characteristics of the target. In this light, our approximation (5) can also be viewed as an interpolation between two limiting regimes. However, its derivation and high accuracy suggest that Eq. (5) correctly represents the dependence of the principal eigenvalue on the main parameters of the problem, at least for small targets.

The third and last result concerns the target anisotropy, which was mainly ignored in former studies. We obtained the exact relations for the trapping length of both prolate and oblate spheroids in $\mathbb{R}^d$ with $d \geqslant 3$ (an extension to more general biaxial ellipsoids is discussed in Appendix C). We showed that the trapping length L vanishes as an elongated target gets thinner. As such a target is hardly accessible to Brownian motion, one might expect to deal with the diffusion-limited regime. However, the vanishing of L implies that diffusion-controlled reactions on needlelike targets are always in the reaction-limited regime. In other words, even though it is hard to find such a target for the first time, it is even more difficult to retrieve the target after each failed attempt to react. In contrast, the trapping capacity of flattened (disklike) targets is not significantly different from that of round ones.

Our approximation is valid for any space dimension $d \geqslant 3$, and its accuracy gets higher as d grows. It is therefore natural to ask what happens in the planar case ($d = 2$), which stands apart for several reasons. In fact, the recurrent nature of Brownian motion in the plane drastically changes many diffusive properties as compared to higher-dimensional settings, for which Brownian motion is transient. First, a steady-state solution of Eq. (8) that defined the harmonic capacity does not exist for unbounded planar domains. This can be easily seen by considering a disk-shaped capacitor $\mathcal{C}$, for which the problem (8) does not depend on the angular coordinate. A general radial solution of the Laplace equation in polar coordinates, $\Delta u = \frac{1}{r}\partial_r r \partial_r u = 0$, has a form $c_1 + c_2 \ln r$, and there is no way to choose arbitrary constants c_1 and c_2 to get $u(r) \to 0$ as $r \to \infty$, except for the trivial solution with $c_1 = c_2 = 0$. In particular, the probability of capture $\Psi(\boldsymbol{x})$ is always equal to 1 for planar domains. This particular issue can be resolved by replacing the harmonic capacity by the logarithmic capacity [98]. The related asymptotic analysis was realized in earlier works (see [30–34] and references therein); in particular, an expansion of the principal eigenvalue in powers of $\nu = 1/\ln(\varepsilon)$ was derived, where ε is the relative size of the target. The major difference from higher-dimensional settings is a very weak logarithmic dependence of the expansion parameter ν on the relative target size ε so that the leading order of the expansion is usually inaccurate, except for extremely small targets. In other words, one needs to deal with an expansion that contains many terms that are not easily accessible and depends on various geometric properties of the confining domain and the target. More generally, the logarithmic form of the fundamental solution of the Laplace equation in the plane, $-\ln(|\boldsymbol{x} - \boldsymbol{x}'|)/(2\pi)$, is responsible for "long-range interactions" between distant points of space such as, for instance, the strong impact of an outer boundary onto the behavior near the target. This fundamental difference makes our approach less useful in the plane.

The present work has several perspectives and possible extensions. First, it would be interesting to rederive the approximation (5) in a more rigorous way and/or by a direct analysis of the eigenvalue problem, e.g., by matched asymptotic methods. In fact, our derivation involved three approximations, and it was difficult to control the accuracy and relevance of each step. Second, one can deal with multiple small targets. If the sizes of the targets are much smaller than the distances between them and from the outer reflecting boundary, the approximation (5) is expected to hold. Note that the capacity of the union of small targets is equal, in leading order, to the sum of their capacities; the surface area is also additive. Moreover, Cheviakov and Ward derived the next-order correction term to the principal eigenvalue for a configuration of perfect targets [40]. This correction term can be used to define the "corrected" capacity C', as we did in Eq. (16) for a single target. A numerical validation of this approximation in configurations with multiple targets presents an important perspective. When the targets are spherical, one can apply efficient semianalytical methods based on addition theorems (see [106,107] and references therein). Another validation step concerns irregularly shaped targets, whose surface area and thus the trapping length can be (arbitrarily) large, despite their smallness. Such a situation is not possible for spheroids, for which $L \leqslant b/(d-2)$ (see Fig. 4), i.e., the smallness of the target diameter $2b$ implied the smallness of L. The accuracy of our approximation for $L/b \gg 1$ remains to be analyzed. Finally, one can investigate other surface reaction mechanisms (beyond the conventional Robin boundary condition) by using an encounter-based approach [27,89,90,92]. Here, the explicit dependence of the reactivity parameter q may allow us to access various properties of diffusion-mediated surface phenomena.

ACKNOWLEDGMENT

D.S.G. acknowledges the Alexander von Humboldt Foundation for support within a Bessel Prize award.

APPENDIX A: PROLATE SPHEROIDS

The harmonic capacity and the surface area of general ellipsoids in $\mathbb{R}^d$ with $d > 3$ have been studied in [103]. Here we describe the main derivation steps and further simplifications that we managed to get for prolate spheroids defined by Eq. (40), with $d-1$ minor semiaxes a and one major semiaxis b such as $a < b$. Combining the standard prolate spheroidal coordinates in $\mathbb{R}^3$ with multidimensional spherical coordinates, one can introduce the following d-dimensional spheroidal coordinates:

$$\begin{aligned}
x_d &= c\cosh(\alpha)\cos(\theta_1),\\
x_{d-1} &= c\sinh(\alpha)\sin(\theta_1)\cos(\theta_2),\\
x_{d-2} &= c\sinh(\alpha)\sin(\theta_1)\sin(\theta_2)\cos(\theta_3),\\
&\vdots\\
x_2 &= c\sinh(\alpha)\sin(\theta_1)\cdots\sin(\theta_{d-2})\cos(\phi),\\
x_1 &= c\sinh(\alpha)\sin(\theta_1)\cdots\sin(\theta_{d-2})\sin(\phi),
\end{aligned}$$

where $c = \sqrt{b^2 - a^2}$ is the focal half-distance, $0 < \alpha < \infty$ is analogous to the radial coordinate, whereas $0 \leqslant \theta_i \leqslant \pi$ and $0 \leqslant \phi < 2\pi$ are angular coordinates. Substituting these coordinates in the quadratic equation in Eq. (40), one sets $\cosh(\alpha_0) = b/c$ [and thus $\sinh(\alpha_0) = a/c$] to determine the "radial" coordinate α_0 of the spheroidal boundary $\Gamma_{a,b}$. The following construction is fairly standard in differential geometry [108,109]. In fact, one first determines the basis vectors associated with new coordinates, e.g., the vector $\vec{e}_\alpha = (dx_1/d\alpha, \ldots, dx_d/d\alpha)^\dagger$ is associated with α, etc. The norms of these vectors determine the scale factors:

$$\begin{aligned}
h_\alpha &= h_{\theta_1} = c\sqrt{\sinh^2\alpha + \sin^2\theta_1},\\
h_{\theta_k} &= c\,\sinh\alpha\,\sin\theta_1\cdots\sin\theta_{k-1} \quad (k = 2, 3, \ldots, d-2),\\
h_\phi &= c\,\sinh\alpha\,\sin\theta_1\cdots\sin\theta_{d-2},
\end{aligned}$$

from which follow the metric, volume and surface elements, and the form of the Laplace operator. Skipping these technical details, we write the Laplace operator as

$$\begin{aligned}
\Delta = {}& \frac{1}{c^2(\sinh^2\alpha + \sin^2\theta_1)}\big(\partial_\alpha^2 + (d-2)\coth\alpha\,\partial_\alpha\big)\\
&+ \frac{1}{c^2(\sinh^2\alpha + \sin^2\theta_1)}\big(\partial_{\theta_1}^2 + (d-2)\cot\theta_1\partial_{\theta_1}\big)\\
&+ \frac{1}{c^2\sinh^2\alpha\sin^2\theta_1}\big(\partial_{\theta_2}^2 + (d-3)\cot\theta_2\partial_{\theta_2}\big)\\
&+ \frac{1}{c^2\sinh^2\alpha\sin^2\theta_1\sin^2\theta_2}\big(\partial_{\theta_3}^2 + (d-4)\cot\theta_3\partial_{\theta_3}\big)\\
&+ \cdots\\
&+ \frac{1}{c^2\sinh^2\alpha\sin^2\theta_1\cdots\sin^2\theta_{d-3}}\big(\partial_{\theta_{d-2}}^2 + \cot\theta_{d-2}\partial_{\theta_{d-2}}\big)\\
&+ \frac{1}{c^2\sinh^2\alpha\sin^2\theta_1\cdots\sin^2\theta_{d-2}}\partial_\phi^2. \qquad \text{(A1)}
\end{aligned}$$

To compute the capacity, one needs to solve the Dirichlet boundary value problem:

$$\Delta\Psi(\boldsymbol{x}) = 0 \quad (\boldsymbol{x} \in \mathbb{R}^d\backslash\mathcal{C}), \qquad \begin{cases}\Psi|_{\partial\mathcal{C}} = 1,\\ \lim_{|\boldsymbol{x}|\to\infty}\Psi(\boldsymbol{x}) = 0,\end{cases} \qquad \text{(A2)}$$

where $\mathcal{C}$ is the interior of the prolate spheroid surrounded by $\Gamma_{a,b}$. Since the Dirichlet boundary condition involves a constant, the solution of this problem is invariant under rotations around the coordinate axis x_d. In spheroidal coordinates, the function $\Psi(\boldsymbol{x})$ thus depends only on the "radial" coordinate α so that only the first term in the above Laplace operator remains,

$$\frac{1}{c^2(\sinh^2\alpha + \sin^2\theta_1)}\big(\partial_\alpha^2 + (d-2)\coth\alpha\,\partial_\alpha\big)\Psi(\alpha) = 0. \qquad \text{(A3)}$$

Setting $\xi = \cosh\alpha$, this equation is reduced to

$$(\xi^2 - 1)\partial_\xi^2\Psi + (d-1)\xi\,\partial_\xi\Psi = 0, \qquad \text{(A4)}$$

subject to the Dirichlet boundary condition $\Psi(\xi_0) = 1$ with $\xi_0 = \cosh(\alpha_0) = b/c$ and the regularity condition $\Psi(\xi) \to 0$ as $\xi \to \infty$. Setting $u(\xi) = \partial_\xi\Psi(\xi)$, one integrates Eq. (A4) to get $u(\xi) = c_1(\xi^2 - 1)^{(1-d)/2}$, with an arbitrary constant c_1. The integral of this function yields

$$\Psi(\xi) = c_1\int_\xi^\infty dz\,(z^2 - 1)^{-\eta}, \quad \eta = \frac{d-1}{2}, \qquad \text{(A5)}$$

the form of which ensures the regularity condition. Setting $y = 1/z^2$ and using the Taylor expansion of $(1-y)^{-\eta}$, one can express this integral in terms of the hypergeometric function,

$$\begin{aligned}\Psi(\xi) &= \frac{c_1}{2}\int_0^{1/\xi^2} dy\, y^{\eta-3/2}(1-y)^{-\eta} \\ &= c_1\frac{\xi^{1-2\eta}}{2\eta-1}\,{}_2F_1(\eta,\eta-1/2;\eta+1/2;1/\xi^2) \\ &= c_1\frac{(\xi^2-1)^{1-\eta}}{\xi(2\eta-1)}\,{}_2F_1(1/2,1;\eta+1/2;1/\xi^2).\end{aligned}$$

Substituting $\eta=(d-1)/2$ and $\xi_0=\cosh\alpha_0=b/c$, we determine the constant c_1 from the Dirichlet boundary condition:

$$c_1 = \frac{(d-2)b}{a^{3-d}c^{d-2}\,{}_2F_1(1/2,1;d/2;c^2/b^2)}. \tag{A6}$$

Finally, we need to evaluate the integral of the normal derivative of the solution in Eq. (A5),

$$(\partial_n\Psi)_{|\Gamma_{a,b}} = -\left(\frac{1}{h_\alpha}\partial_\alpha\Psi\right)_{\alpha=\alpha_0}, \tag{A7}$$

over the surface $\Gamma_{a,b}$:

$$\begin{aligned}C_{a,b}^{(d)} &= \int_{\Gamma_{a,b}} d\boldsymbol{x}\,(\partial_n\Psi) \\ &= c^{d-2}[\sinh\alpha_0]^{d-2}\int_0^\pi d\theta_1\,\sin^{d-2}\theta_1\int_0^\pi d\theta_2\,\sin^{d-3}\theta_2 \\ &\quad \cdots\int_0^\pi d\theta_{d-2}\,\sin\theta_{d-2}\int_0^{2\pi} d\phi\,(-\partial_\alpha\Psi)_{\alpha=\alpha_0},\end{aligned} \tag{A8}$$

where the surface element was expressed in terms of the scale factors, and we used that the equal scale factors h_α and h_{θ_1} compensated each other. The integrals over angular coordinates yield the surface area σ_d of the unit sphere in $\mathbb{R}^d$ so that

$$\begin{aligned}C_{a,b}^{(d)} &= \sigma_d c^{d-2}[\sinh\alpha_0]^{d-2}(-\partial_\alpha\Psi)_{\alpha=\alpha_0} = \sigma_d\, c^{d-2}\, c_1 \\ &= \frac{(d-2)\sigma_d\, a^{d-3}\, b}{{}_2F_1(1/2,1;d/2;c^2/b^2)},\end{aligned} \tag{A9}$$

i.e., we arrive at Eq. (42). To our knowledge, such a compact expression for the capacity of the prolate spheroid in $\mathbb{R}^d$ has not been reported.

The surface area of ellipsoids was derived in [103]. In our particular case, the general expression can be written as

$$\left|\Gamma_{a,b}^{(d)}\right| = \frac{4\pi^{(d-1)/2}a^{d-3}b^2}{\Gamma\left(\frac{d-1}{2}\right)}\int_0^1 dx\,\frac{(1-x^2)^{(d-3)/2}}{(1+\delta x^2)^{(d+1)/2}}, \tag{A10}$$

where $\delta=b^2/a^2-1$. This integral can be expressed in terms of the hypergeometric function:

$$\left|\Gamma_{a,b}^{(d)}\right| = \frac{2\pi^{d/2}a^{d-3}b^2}{\Gamma(d/2)}\,{}_2F_1\left(\frac{1}{2},\frac{d+1}{2};\frac{d}{2};1-\frac{b^2}{a^2}\right). \tag{A11}$$

Using the Pfaff transformation, one can rewrite it as Eq. (47).

In three dimensions, one retrieves the classical expression

$$\left|\Gamma_{a,b}^{(3)}\right| = 2\pi a^2\left(1+\frac{b}{ae}\sin^{-1}(e)\right),\qquad e=\sqrt{1-a^2/b^2}, \tag{A12}$$

so that the trapping length reads

$$L = \frac{a^2\left(1+\frac{b}{ae}\sin^{-1}(e)\right)\ln\left(\frac{1+e}{1-e}\right)}{4eb}. \tag{A13}$$

Note that $L\approx a\frac{\pi}{4}\ln(2b/a)$ as $a\to 0$.

APPENDIX B: OBLATE SPHEROIDS

The derivation for oblate spheroids is very similar. One introduces an extension of the oblate spheroidal coordinates as

$$\begin{aligned}x_d &= c\sinh(\alpha)\sin(\theta_1),\\ x_{d-1} &= c\cosh(\alpha)\cos(\theta_1)\sin(\theta_2),\\ x_{d-2} &= c\cosh(\alpha)\cos(\theta_1)\cos(\theta_2)\sin(\theta_3),\\ &\vdots\\ x_2 &= c\cosh(\alpha)\cos(\theta_1)\cdots\cos(\theta_{d-2})\sin(\phi),\\ x_1 &= c\cosh(\alpha)\cos(\theta_1)\cdots\cos(\theta_{d-2})\cos(\phi),\end{aligned}$$

with $c=\sqrt{b^2-a^2}$, $0<\alpha<\infty$, $-\pi/2\leqslant\theta_i\leqslant\pi/2$, and $0\leqslant\phi<2\pi$. These coordinates determine the scale factors

$$\begin{aligned}h_\alpha &= h_{\theta_1} = c\sqrt{\sinh^2\alpha+\sin^2\theta_1},\\ h_{\theta_k} &= c\,\cosh\alpha\,\cos\theta_1\cdots\cos\theta_{k-1}\quad (k=2,3,\dots,d-2),\\ h_\phi &= c\,\cosh\alpha\,\cos\theta_1\cdots\cos\theta_{d-2},\end{aligned}$$

from which the metric and the Laplace operator follow. In particular, the solution of the boundary value problem (A2) depends only on the "radial coordinate" α:

$$\frac{1}{c^2(\sinh^2\alpha+\sin^2\theta_1)}\left(\partial_\alpha^2+(d-2)\tanh\alpha\,\partial_\alpha\right)\Psi(\alpha)=0. \tag{B1}$$

Setting $\xi=\sinh\alpha$, this equation is reduced to

$$(\xi^2+1)\partial_\xi^2\Psi+(d-1)\xi\,\partial_\xi\Psi=0, \tag{B2}$$

subject to the Dirichlet boundary condition $\Psi(\xi_0)=1$ with $\xi_0=\sinh(\alpha_0)=a/c$ and the regularity condition $\Psi(\xi)\to 0$ as $\xi\to\infty$. Setting $u(\xi)=\partial_\xi\Psi(\xi)$, one gets $u(\xi)=c_1(\xi^2+1)^{(1-d)/2}$, with an arbitrary constant c_1. The integral of this function yields

$$\Psi(\xi)=c_1\int_\xi^\infty dz\,(z^2+1)^{-\eta},\qquad \eta=\frac{d-1}{2}. \tag{B3}$$

As was done previously, one can express this solution as

$$\begin{aligned}\Psi(\xi) &= \frac{c_1}{2}\int_0^{1/\xi^2} dy\, y^{\eta-3/2}(1+y)^{-\eta} \\ &= c_1\frac{\xi^{1-2\eta}}{2\eta-1}\,{}_2F_1(\eta,\eta-1/2;\eta+1/2;-1/\xi^2) \\ &= c_1\frac{(\xi^2+1)^{1-\eta}}{\xi(2\eta-1)}\,{}_2F_1(1/2,1;\eta+1/2;-1/\xi^2).\end{aligned} \tag{B4}$$

Substituting $\eta=(d-1)/2$ and $\xi_0=\sinh(\alpha_0)=a/c$, we get

$$c_1 = \frac{(d-2)a}{b^{3-d}c^{d-2}\,{}_2F_1(1/2,1;d/2;-c^2/a^2)}. \tag{B5}$$

To complete the computation, we need to evaluate the integral of the normal derivative of this solution,

$$(\partial_n \Psi)_{|\tilde{\Gamma}_{a,b}} = -\left(\frac{1}{h_\alpha}\partial_\alpha \Psi\right)_{\alpha=\alpha_0}, \tag{B6}$$

over the surface $\tilde{\Gamma}_{a,b}$:

$$\begin{aligned}\tilde{C}_{a,b}^{(d)} &= \int_{\tilde{\Gamma}_{a,b}} d\boldsymbol{x}\,(\partial_n \Psi)\\ &= c^{d-2}[\cosh\alpha_0]^{d-2}\int_{-\pi/2}^{\pi/2} d\theta_1\,\cos^{d-2}\theta_1\int_{-\pi/2}^{\pi/2} d\theta_2\,\cos^{d-3}\theta_2\\ &\quad\cdots\int_{-\pi/2}^{\pi/2} d\theta_{d-2}\,\cos\theta_{d-2}\int_0^{2\pi} d\phi\,(-\partial_\alpha\Psi)_{\alpha=\alpha_0}.\end{aligned} \tag{B7}$$

Evaluating the integrals over angular coordinates, we get

$$\begin{aligned}\tilde{C}_{a,b}^{(d)} &= \sigma_d c^{d-2}[\cosh\alpha_0]^{d-2}(-\partial_\alpha\Psi)_{\alpha=\alpha_0} = \sigma_d\, c^{d-2}\, c_1\\ &= \frac{(d-2)\sigma_d\, a\, b^{d-3}}{{}_2F_1(1/2, 1; d/2; -c^2/a^2)}.\end{aligned} \tag{B8}$$

Using the Pfaff transformation, one can rewrite this expression as Eq. (53). To our knowledge, such a compact expression for the capacity of the oblate spheroid in $\mathbb{R}^d$ has not been reported.

The surface area of oblate spheroids is given by the formula (A11), in which a and b are exchanged:

$$\left|\tilde{\Gamma}_{a,b}^{(d)}\right| = \sigma_d\, b^{d-3}a^2\, {}_2F_1\left(\frac{1}{2}, \frac{d+1}{2}; \frac{d}{2}; 1-\frac{a^2}{b^2}\right). \tag{B9}$$

Using the Euler transformation, one gets a more convenient representation (57).

In three dimensions, one retrieves the classical formula

$$\left|\tilde{\Gamma}_{a,b}^{(3)}\right| = 2\pi b^2 + \pi\frac{a^2}{e}\ln\frac{1+e}{1-e}. \tag{B10}$$

The trapping length is

$$L = \frac{2\pi b^2 + \pi\frac{a^2}{e}\ln\frac{1+e}{1-e}}{4\pi c}\cos^{-1}(a/b). \tag{B11}$$

APPENDIX C: BIAXIAL ELLIPSOIDS

The prolate and oblate spheroids discussed in Appendixes A and B are particular cases of a biaxial ellipsoid, which has p minor semiaxes a and q major semiaxes b (such that $a < b$). For the sake of completeness, we provide here the exact expressions for the capacity and the surface area of these domains. We recast former results by Tee in [103] in a simpler form in terms of hypergeometric functions.

Tee obtained the following formula for the capacity of a biaxial ellipsoid with p minor semiaxes a and q major semiaxes $b > a$:

$$\frac{1}{C} = \frac{1}{b^{p+q-2}\sigma_{p+q}}\int_0^1 dx\frac{x^{p+q-3}}{(1-(1-a^2/b^2)x^2)^{p/2}}, \tag{C1}$$

where σ_d is given by Eq. (10). Expanding the denominator into a Taylor series of powers of x, we get

$$C = \frac{(p+q-2)\sigma_{p+q}b^{p+q-2}}{{}_2F_1\left(\frac{p}{2}, \frac{p+q-2}{2}; \frac{p+q}{2}; 1-a^2/b^2\right)}. \tag{C2}$$

The Euler transformation allows one to get another representation:

$$C = \frac{(p+q-2)\sigma_{p+q}a^{p-2}b^q}{{}_2F_1\left(\frac{q}{2}, 1; \frac{p+q}{2}; 1-a^2/b^2\right)}. \tag{C3}$$

For instance, inserting $p = d-1$ and $q = 1$ into the last formula, we retrieve Eq. (A9) for a prolate spheroid in $\mathbb{R}^d$. Similarly, inserting $p = 1$ and $q = d-1$ into Eq. (C2) yields Eq. (53) for an oblate spheroid.

Tee expressed the surface area of biaxial ellipsoids in terms of the integrals

$$I_{\alpha,\beta}(\delta) = \int_0^1 dh\,\frac{(1-h^2)^\alpha}{(1-\delta h^2)^\beta}. \tag{C4}$$

Setting $\mu = \delta/(\delta-1)$ and using the Taylor expansion of $(1-\mu x)^{-\beta}$, we have

$$\begin{aligned}I_{\alpha,\beta}(\delta) &= \frac{1}{2(1-\delta)^\beta}\int_0^1 \frac{dx}{\sqrt{1-x}}\,\frac{x^\alpha}{(1-\mu x)^\beta}\\ &= \frac{\sqrt{\pi}\,\Gamma(\alpha+1)}{2(1-\delta)^\beta\Gamma\left(\alpha+\frac{3}{2}\right)}\,{}_2F_1\left(\beta, \alpha+1; \alpha+\frac{3}{2}; \frac{\delta}{\delta-1}\right),\end{aligned} \tag{C5}$$

where we used

$$\int_0^1 dx\frac{x^\alpha}{\sqrt{1-x}} = \frac{\sqrt{\pi}\,\Gamma(\alpha+1)}{\Gamma(\alpha+3/2)}.$$

Depending on the parity of p and q, Tee treated separately three cases and expressed the surface area of the corresponding biaxial ellipsoids in terms of $I_{\alpha,\beta}(\delta)$, with α and β being related to p and q. Using Eq. (C5), we managed to show that all three cases yield the same result. Skipping the technical details of this analysis, we provide the following exact expression for the surface area:

$$\begin{aligned}|\Gamma| &= \frac{\sigma_{p+q}a^{p-1}b^q}{p+q-1}\left\{\frac{(q-1)a^2}{b^2}\,{}_2F_1\left(\frac{1}{2}, \frac{q}{2}; \frac{p+q}{2}; 1-\frac{a^2}{b^2}\right)\right.\\ &\quad\left.+\, p\,{}_2F_1\left(\frac{1}{2}, \frac{q}{2}-1; \frac{p+q}{2}; 1-\frac{a^2}{b^2}\right)\right\}.\end{aligned} \tag{C6}$$

For a prolate spheroid with $q = 1$ and $p = d-1$, we retrieve Eq. (47). For an oblate spheroid with $q = d-1$ and $p = 1$, one can use contiguous relations between hypergeometric functions to retrieve Eq. (57).

Substituting Eqs. (C2) or (C3) for C and Eq. (C6) for $|\Gamma|$ into Eq. (6), one determines the trapping length of a general biaxial ellipsoid.

APPENDIX D: NUMERICAL SOLUTION BY THE FINITE-ELEMENTS METHOD

To check the accuracy of our approximation, we solved the underlying boundary value problem using a finite-elements method. The axial symmetry of spheroids allowed us to reduce the original d-dimensional problem to a planar one. In fact, one can write the Laplace operator in the cylindrical coordinates as

$$\Delta = \partial_z^2 + \frac{1}{r^{d-2}}\partial_r\, r^{d-2}\,\partial_r + \frac{1}{r^2}\Delta_{\text{ang}}, \tag{D1}$$

where z denotes the coordinate along the symmetry axis (i.e., $z = x_d$), $r = \sqrt{x_1^2 + \cdots + x_{d-1}^2}$, and Δ_{ang} is the angular part of the Laplace operator in the hyperplane $\mathbb{R}^{d-1}$, which is orthogonal to the axis x_d. As the original eigenvalue problem in Eq. (4a) is invariant under rotations along the x_d axis, its solution does not depend on the angular part. It can thus be written as

$$-\nabla c \nabla u = \lambda r^{d-2} u, \tag{D2}$$

where ∇ is the gradient operator in the (r, z) plane, and c is the diagonal 2×2 matrix with entries r^{d-2}. This reduced eigenvalue problem has to be solved in the planar cross section of the domain (see Fig. 6). The problem was solved numerically by PDETool in MATLAB. We compared numerical solutions with different choices for the maximal mesh size to ensure that the results do not depend on this choice.

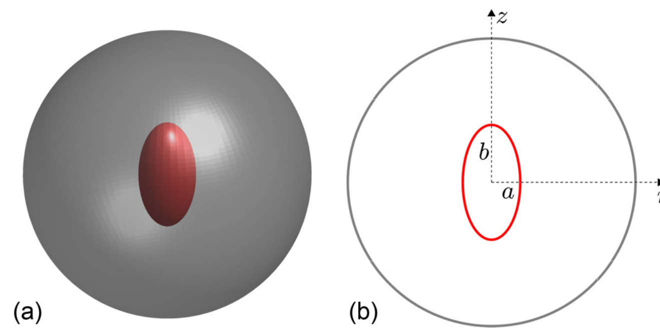

FIG. 6. (a) A prolate spheroidal target (in red) is enclosed by an outer reflecting sphere (in gray). (b) An equivalent planar domain with an elliptic target (in red) and an outer circular reflecting boundary (in gray).

[1] S. Rice, *Diffusion-Limited Reactions* (Elsevier, Amsterdam, 1985).
[2] D. A. Lauffenburger and J. Linderman, *Receptors: Models for Binding, Trafficking, and Signaling* (Oxford University Press, Oxford, 1993).
[3] S. Redner, *A Guide to First Passage Processes* (Cambridge University Press, Cambridge, 2001).
[4] Z. Schuss, *Brownian Dynamics at Boundaries and Interfaces in Physics, Chemistry and Biology* (Springer, New York, 2013).
[5] *First-Passage Phenomena and Their Applications*, edited by R. Metzler, G. Oshanin, and S. Redner (World Scientific, Singapore, 2014).
[6] *Chemical Kinetics: Beyond the Textbook*, edited by K. Lindenberg, R. Metzler, and G. Oshanin (World Scientific, New Jersey, 2019).
[7] D. S. Grebenkov, NMR survey of reflected Brownian motion, Rev. Mod. Phys. **79**, 1077 (2007).
[8] O. Bénichou, C. Loverdo, M. Moreau, and R. Voituriez, Intermittent search strategies, Rev. Mod. Phys. **83**, 81 (2011).
[9] P. C. Bressloff and J. M. Newby, Stochastic models of intracellular transport, Rev. Mod. Phys. **85**, 135 (2013).
[10] O. Bénichou and R. Voituriez, From first-passage times of random walks in confinement to geometry-controlled kinetics, Phys. Rep. **539**, 225 (2014).
[11] F. C. Collins and G. E. Kimball, Diffusion-controlled reaction rates, J. Colloid Sci. **4**, 425 (1949).
[12] H. C. Berg and E. M. Purcell, Physics of chemoreception, Biophys. J. **20**, 193 (1977).
[13] H. Sano and M. Tachiya, Partially diffusion-controlled recombination, J. Chem. Phys. **71**, 1276 (1979).
[14] G. H. Weiss, Overview of theoretical models for reaction rates, J. Stat. Phys. **42**, 3 (1986).
[15] S. Condamin, O. Bénichou, V. Tejedor, R. Voituriez, and J. Klafter, First-passage time in complex scale-invariant media, Nature (London) **450**, 77 (2007).
[16] O. Bénichou and R. Voituriez, Narrow-Escape Time Problem: Time Needed for a Particle to Exit a Confining Domain through a Small Window, Phys. Rev. Lett. **100**, 168105 (2008).
[17] O. Bénichou, D. S. Grebenkov, P. Levitz, C. Loverdo, and R. Voituriez, Optimal Reaction Time for Surface-Mediated Diffusion, Phys. Rev. Lett. **105**, 150606 (2010).
[18] O. Bénichou, C. Chevalier, J. Klafter, B. Meyer, and R. Voituriez, Geometry-controlled kinetics, Nat. Chem. **2**, 472 (2010).
[19] J.-F. Rupprecht, O. Benichou, D. S. Grebenkov, and R. Voituriez, Exit time distribution in spherically symmetric two-dimensional domains, J. Stat. Phys. **158**, 192 (2015).
[20] A. Godec and R. Metzler, First passage time distribution in heterogeneity controlled kinetics: Going beyond the mean first passage time, Sci. Rep. **6**, 20349 (2016).
[21] A. Godec and R. Metzler, Universal Proximity Effect in Target Search Kinetics in the Few-Encounter Limit, Phys. Rev. X **6**, 041037 (2016).
[22] J. S. Marshall, Analytical solutions for an escape problem in a disc with an arbitrary distribution of exit holes along its boundary, J. Stat. Phys. **165**, 920 (2016).
[23] D. S. Grebenkov, Universal Formula for the Mean First Passage Time in Planar Domains, Phys. Rev. Lett. **117**, 260201 (2016).
[24] A. V. Chechkin, F. Seno, R. Metzler, and I. M. Sokolov, Brownian Yet Non-Gaussian Diffusion: From Superstatistics to Subordination of Diffusing Diffusivities, Phys. Rev. X **7**, 021002 (2017).
[25] Y. Lanoiselée, N. Moutal, and D. S. Grebenkov, Diffusion-limited reactions in dynamic heterogeneous media, Nat. Commun. **9**, 4398 (2018).
[26] N. Levernier, M. Dolgushev, O. Bénichou, R. Voituriez, and T. Guérin, Survival probability of stochastic processes beyond persistence exponents, Nat. Commun. **10**, 2990 (2019).
[27] D. S. Grebenkov, Paradigm Shift in Diffusion-Mediated Surface Phenomena, Phys. Rev. Lett. **125**, 078102 (2020).
[28] C. W. Gardiner, *Handbook of Stochastic Methods for Physics, Chemistry and the Natural Sciences* (Springer, Berlin, 1985).
[29] D. S. Grebenkov, R. Metzler, and G. Oshanin, Strong defocusing of molecular reaction times results from an interplay of geometry and reaction control, Commun. Chem. **1**, 96 (2018).

[30] S. Ozawa, Singular variation of domains and eigenvalues of the Laplacian, Duke Math. J. **48**, 767 (1981).
[31] V. G. Maz'ya, S. A. Nazarov, and B. A. Plamenevskii, Asymptotic expansions of the eigenvalues of boundary value problems for the laplace operator in domains with small holes, Math. USSR Izv. **24**, 321 (1985).
[32] M. J. Ward and J. B. Keller, Strong localized perturbations of eigenvalue problems, SIAM J. Appl. Math. **53**, 770 (1993).
[33] M. J. Ward, W. D. Henshaw, and J. B. Keller, Summing logarithmic expansions for singularly perturbed eigenvalue problems, SIAM J. Appl. Math. **53**, 799 (1993).
[34] T. Kolokolnikov, M. S. Titcombe, and M. J. Ward, Optimizing the fundamental neumann eigenvalue for the laplacian in a domain with small traps, Eur. J. Appl. Math. **16**, 161 (2005).
[35] A. Singer, Z. Schuss, D. Holcman, and R. S. Eisenberg, Narrow escape, Part I, J. Stat. Phys. **122**, 437 (2006).
[36] A. Singer, Z. Schuss, and D. Holcman, Narrow escape, Part II. The circular disk, J. Stat. Phys. **122**, 465 (2006).
[37] A. Singer, Z. Schuss, and D. Holcman, Narrow escape, Part III. Riemann surfaces and non-smooth domains, J. Stat. Phys. **122**, 491 (2006).
[38] S. Pillay, M. J. Ward, A. Peirce, and T. Kolokolnikov, An asymptotic analysis of the mean first passage time for narrow escape problems: Part I: Two-dimensional domains, SIAM Multi. Model. Simul. **8**, 803 (2010).
[39] A. F. Cheviakov, M. J. Ward, and R. Straube, An asymptotic analysis of the mean first passage time for narrow escape problems: Part II: The sphere, SIAM Multi. Model. Simul. **8**, 836 (2010).
[40] A. F. Cheviakov and M. J. Ward, Optimizing the principal eigenvalue of the Laplacian in a sphere with interior traps, Math. Comput. Model. **53**, 1394 (2011).
[41] A. F. Cheviakov, A. S. Reimer, and M. J. Ward, Mathematical modeling and numerical computation of narrow escape problems, Phys. Rev. E **85**, 021131 (2012).
[42] D. Holcman and Z. Schuss, The narrow escape problem, SIAM Rev. **56**, 213 (2014).
[43] S. A. Isaacson and J. Newby, Uniform asymptotic approximation of diffusion to a small target, Phys. Rev. E **88**, 012820 (2013).
[44] R. Zwanzig, Diffusion-controlled ligand binding to spheres partially covered by receptors: An effective medium treatment, Proc. Natl. Acad. Sci. (USA) **87**, 5856 (1990).
[45] I. V. Grigoriev, Y. A. Makhnovskii, A. M. Berezhkovskii, and V. Y. Zitserman, Kinetics of escape through a small hole, J. Chem. Phys. **116**, 9574 (2002).
[46] A. Berezhkovskii, Y. Makhnovskii, M. Monine, V. Zitserman, and S. Shvartsman, Boundary homogenization for trapping by patchy surfaces, J. Chem. Phys. **121**, 11390 (2004).
[47] A. M. Berezhkovskii, M. I. Monine, C. B. Muratov, and S. Y. Shvartsman, Homogenization of boundary conditions for surfaces with regular arrays of traps, J. Chem. Phys. **124**, 036103 (2006).
[48] C. Muratov and S. Shvartsman, Boundary homogenization for periodic arrays of absorbers, Multiscale Model. Simul. **7**, 44 (2008).
[49] L. Dagdug, M. Vázquez, A. Berezhkovskii, and V. Zitserman, Boundary homogenization for a sphere with an absorbing cap of arbitrary size, J. Chem. Phys. **145**, 214101 (2016).
[50] A. E. Lindsay, A. J. Bernoff, and M. J. Ward, First passage statistics for the capture of a brownian particle by a structured spherical target with multiple surface traps, Multiscale Model. Simul. **15**, 74 (2017).
[51] A. J. Bernoff and A. E. Lindsay, Numerical approximation of diffusive capture rates by planar and spherical surfaces with absorbing pores, SIAM J. Appl. Math. **78**, 266 (2018).
[52] A. Bernoff, A. Lindsay, and D. Schmidt, Boundary homogenization and capture time distributions of semipermeable membranes with periodic patterns of reactive sites, Multiscale Model. Simul. **16**, 1411 (2018).
[53] D. S. Grebenkov, Spectral theory of imperfect diffusion-controlled reactions on heterogeneous catalytic surfaces, J. Chem. Phys. **151**, 104108 (2019).
[54] D. S. Grebenkov and G. Oshanin, Diffusive escape through a narrow opening: New insights into a classic problem, Phys. Chem. Chem. Phys. **19**, 2723 (2017).
[55] D. S. Grebenkov, R. Metzler, and G. Oshanin, Effects of the target aspect ratio and intrinsic reactivity onto diffusive search in bounded domains, New J. Phys. **19**, 103025 (2017).
[56] D. S. Grebenkov, R. Metzler, and G. Oshanin, Towards a full quantitative description of single-molecule reaction kinetics in biological cells, Phys. Chem. Chem. Phys. **20**, 16393 (2018).
[57] D. S. Grebenkov, R. Metzler, and G. Oshanin, Full distribution of first exit times in the narrow escape problem, New J. Phys. **21**, 122001 (2019).
[58] D. S. Grebenkov, R. Metzler, and G. Oshanin, Distribution of first-reaction times with target regions on boundaries of shell-like domains, New J. Phys. **23**, 123049 (2021).
[59] D. S. Grebenkov and A. T. Skvortsov, Mean first-passage time to a small absorbing target in an elongated planar domain, New J. Phys. **22**, 113024 (2020).
[60] D. S. Grebenkov and A. T. Skvortsov, Mean first-passage time to a small absorbing target in three-dimensional elongated domains, Phys. Rev. E **105**, 054107 (2022).
[61] R. Samson and J. M. Deutch, Exact solution for the diffusion controlled rate into a pair of reacting sinks, J. Chem. Phys. **67**, 847 (1977).
[62] R. I. Cukier, Diffusion-controlled reactions with ellipsoids: Effective medium theory, J. Phys. Chem. **89**, 246 (1985).
[63] O. G. Berg and P. H. von Hippel, Diffusion-controlled macromolecular interactions, Annu. Rev. Biophys. Biophys. Chem. **14**, 131 (1985).
[64] H.-K. Tsao, Competitive diffusion into two reactive spheres of different reactivity and size, Phys. Rev. E **66**, 011108 (2002).
[65] N. McDonald and W. Strieder, Competitive interaction between two different spherical sinks, J. Chem. Phys. **121**, 7966 (2004).
[66] A. M. Berezhkovskii and A. V. Barzykin, Simple formulas for the trapping rate by nonspherical absorber and capacitance of nonspherical conductor, J. Chem. Phys. **126**, 106102 (2007).
[67] M. Galanti, D. Fanelli, S. D. Traytak, and F. Piazza, Theory of diffusion-influenced reactions in complex geometries, Phys. Chem. Chem. Phys. **18**, 15950 (2016).
[68] S. D. Traytak and D. S. Grebenkov, Diffusion-influenced reaction rates for active "sphere-prolate spheroid" pairs and Janus dimers, J. Chem. Phys. **148**, 024107 (2018).
[69] D. R. Grimes and F. J. Currell, Oxygen diffusion in ellipsoidal tumour spheroids, J. R. Soc. Interface **15**, 20180256 (2018).

[70] D. S. Grebenkov and D. Krapf, Steady-state reaction rate of diffusion-controlled reactions in sheets, J. Chem. Phys. **149**, 064117 (2018).
[71] F. Piazza and D. S. Grebenkov, Diffusion-controlled reaction rate on non-spherical partially absorbing axisymmetric surfaces, Phys. Chem. Chem. Phys. **21**, 25896 (2019).
[72] H. Sano and M. Tachiya, Theory of diffusion-controlled reactions on spherical surfaces and its application to reactions on micellar surfaces, J. Chem. Phys. **75**, 2870 (1981).
[73] D. Shoup and A. Szabo, Role of diffusion in ligand binding to macromolecules and cell-bound receptors, Biophys. J. **40**, 33 (1982).
[74] B. Sapoval, General Formulation of Laplacian Transfer Across Irregular Surfaces, Phys. Rev. Lett. **73**, 3314 (1994).
[75] M. Filoche and B. Sapoval, Can one hear the shape of an electrode? II. theoretical study of the laplacian transfer, Eur. Phys. J. B **9**, 755 (1999).
[76] O. Bénichou, M. Moreau, and G. Oshanin, Kinetics of stochastically gated diffusion-limited reactions and geometry of random walk trajectories, Phys. Rev. E **61**, 3388 (2000).
[77] B. Sapoval, M. Filoche, and E. Weibel, Smaller is better—but not too small: A physical scale for the design of the mammalian pulmonary acinus, Proc. Natl. Acad. Sci. (USA) **99**, 10411 (2002).
[78] D. S. Grebenkov, M. Filoche, and B. Sapoval, Spectral properties of the brownian self-transport operator, Eur. Phys. J. B **36**, 221 (2003).
[79] D. S. Grebenkov, M. Filoche, B. Sapoval, and M. Felici, Diffusion-Reaction in Branched Structures: Theory and Application to the Lung Acinus, Phys. Rev. Lett. **94**, 050602 (2005).
[80] D. S. Grebenkov, M. Filoche, and B. Sapoval, Mathematical basis for a general theory of Laplacian transport towards irregular interfaces, Phys. Rev. E **73**, 021103 (2006).
[81] D. S. Grebenkov, Partially reflected brownian motion: A stochastic approach to transport phenomena, in *Focus on Probability Theory*, edited by L. R. Velle (Nova Science, New York, 2006), pp. 135–169.
[82] S. D. Traytak and W. Price, Exact solution for anisotropic diffusion-controlled reactions with partially reflecting conditions, J. Chem. Phys. **127**, 184508 (2007).
[83] P. C. Bressloff, B. A. Earnshaw, and M. J. Ward, Diffusion of protein receptors on a cylindrical dendritic membrane with partially absorbing traps, SIAM J. Appl. Math. **68**, 1223 (2008).
[84] A. Singer, Z. Schuss, Osipov, and D. Holcman, Partially reflected diffusion, SIAM J. Appl. Math. **68**, 844 (2008).
[85] D. S. Grebenkov, Searching for partially reactive sites: Analytical results for spherical targets, J. Chem. Phys. **132**, 034104 (2010).
[86] D. S. Grebenkov, Subdiffusion in a bounded domain with a partially absorbing-reflecting boundary, Phys. Rev. E **81**, 021128 (2010).
[87] S. D. Lawley and J. P. Keener, A new derivation of robin boundary conditions through homogenization of a stochastically switching boundary, SIAM J. Appl. Dyn. Syst. **14**, 1845 (2015).
[88] D. S. Grebenkov, Analytical representations of the spread harmonic measure density, Phys. Rev. E **91**, 052108 (2015).
[89] D. S. Grebenkov, Surface hopping propagator: An alternative approach to diffusion-influenced reactions, Phys. Rev. E **102**, 032125 (2020).
[90] D. S. Grebenkov, Joint distribution of multiple boundary local times and related first-passage time problems with multiple targets, J. Stat. Mech. (2020) 103205.
[91] F. Le Vot, S. B. Yuste, E. Abad, and D. S. Grebenkov, First-encounter time of two diffusing particles in confinement, Phys. Rev. E **102**, 032118 (2020).
[92] D. S. Grebenkov, An encounter-based approach for restricted diffusion with a gradient drift, J. Phys. A **55**, 045203 (2022).
[93] J. D. Jackson, *Classical Electrodynamic*, 3rd ed. (Wiley, New York, 1999).
[94] L. D. Landau, L. P. Pitaevskii, and E. M. Lifshitz, *Electrodynamics of Continuous Media* (Pergamon Press, Oxford, 1984).
[95] N. Landkof, *Foundations of Modern Potential Theory* (Springer-Verlag, Berlin, 1972).
[96] A. A. Samarskii, The influence of anchoring on the natural frequencies of closed volumes, Dokl. Akad. Nauk SSSR **63**, 631 (1948) (in Russian).
[97] D. S. Grebenkov and B.-T. Nguyen, Geometrical structure of Laplacian eigenfunctions, SIAM Rev. **55**, 601 (2013).
[98] J. B. Garnett and D. E. Marshall, *Harmonic Measure* (Cambridge University Press, Cambridge, 2005).
[99] R. M. Noyes, Effects of diffusion rates on chemical kinetics, in *Progress in Reaction Kinetics*, edited by G. Porter (Pergamon, New York, 1961), Vol. 1, pp. 129–160.
[100] D. S. Grebenkov and A. Kumar (unpublished).
[101] D. S. Grebenkov, R. Metzler, and G. Oshanin, From single-particle stochastic kinetics to macroscopic reaction rates: fastest first-passage time of N random walkers, New J. Phys. **22**, 103004 (2020).
[102] A. Lejay and S. Maire, Computing the principal eigenvalue of the Laplace operator by a stochastic method, Math. Comput. Simul. **73**, 351 (2007).
[103] G. J. Tee, Surface area and capacity of ellipsoids in n dimensions, New Zealand J. Math. **34**, 165 (2005).
[104] D. S. Grebenkov, Scaling properties of the spread harmonic measures, Fractals **14**, 231 (2006).
[105] M. Smoluchowski, Versuch einer matematischen theorie der koagulationskinetik kolloider lösungen, Z. Phys. Chem. **92U**, 129 (1918).
[106] D. S. Grebenkov and S. Traytak, Semi-analytical computation of Laplacian Green functions in three-dimensional domains with disconnected spherical boundaries, J. Comput. Phys. **379**, 91 (2019).
[107] D. S. Grebenkov, Diffusion toward non-overlapping partially reactive spherical traps: Fresh insights onto classic problems, J. Chem. Phys. **152**, 244108 (2020).
[108] B. A. Dubrovin, A. T. Fomenko, and S. P. Novikov, *Modern Geometry: Methods and Applications* (Springer-Verlag, New York, 1984).
[109] M. Berger and B. Gostiaux, *Differential Geometry: Manifolds, Curves, and Surfaces* (Springer-Verlag, New York, 1988).